Strength model for end cover separation failure in RC beams strengthened with near-surface mounted (NSM) FRP strips

Teng, J. G., Zhang, S. S., & Chen, J. F. (2016). Strength model for end cover separation failure in RC beams strengthened with near-surface mounted (NSM) FRP strips. *Engineering Structures*, *110*, 222-232. https://doi.org/10.1016/j.engstruct.2015.11.049

Published in:
Engineering Structures

Document Version:
Peer reviewed version

Strength Model for End Cover Separation Failure in RC Beams Strengthened with Near-Surface Mounted (NSM) FRP Strips

J.G. Teng[1,*], S.S. Zhang[2] and J.F. Chen[3]

[1]Department of Civil and Environmental Engineering, The Hong Kong Polytechnic University, Hong Kong, China. Email: cejgteng@polyu.edu.hk

[2]School of Civil, Mining & Environmental Engineering, Faculty of Engineering & Information Sciences, University of Wollongong, Northfields Avenue, Wollongong, NSW 2522, Australia.

[3]School of Planning, Architecture and Civil Engineering, Queen's University Belfast, Belfast BT9 5AG, UK

Abstract: As an alternative to externally bonded FRP reinforcement, near-surface mounted (NSM) FRP reinforcement can be used to effectively improve the flexural performance of RC beams. In such FRP-strengthened RC beams, end cover separation failure is one of the common failure modes. This failure mode involves the detachment of the NSM FRP reinforcement together with the concrete cover along the level of the tension steel reinforcement. This paper presents a new strength model for end cover separation failure in RC beams strengthened in flexure with NSM FRP strips (i.e. rectangular FRP bars with a sectional height-to-thickness ratio not less than 5), which was formulated on the basis of extensive numerical results from a parametric study undertaken using an efficient finite element approach. The proposed strength model consists of an approximate equation for the debonding strain of the FRP reinforcement at the critical cracked section and a conventional section analysis to relate this debonding strain to the moment acting on the same section (i.e. the debonding strain). Once the debonding strain is known, the load level at end cover separation of an FRP-strengthened RC beam can be easily determined for a given load distribution. Predictions from the proposed strength model are compared with those of two existing strength models of the same type and available test results, which shows that the proposed strength model is in close agreement with test results and is far more accurate than the existing strength models.

Keywords: End cover separation, finite element analysis, FRP strengthening, near-surface mounted (NSM) FRP, RC beams, strength model

* Corresponding author. Email: cejgteng@polyu.edu.hk; Fax: +852 2766 1354; Tel: +852 2766 6012

1 Introduction

Extensive research has been undertaken on the flexural strengthening of reinforced concrete (RC) beams using bonded FRP reinforcement. Strengthening using externally bonded FRP reinforcement has received by far the largest amount of research [1-5], but the alternative of near-surface mounted (NSM) FRP reinforcement has also received increasing attention [e.g. 6-11]. The externally bonded FRP method involves the external bonding of FRP laminates, either formed in-situ via the wet layup process or prefabricated off site generally by pultrusion, to the tension surface of RC members. The NSM FRP method involves the cutting of grooves in the cover concrete and the embedding of FRP bars in the grooves using an adhesive. FRP bars of various cross-sectional shapes can be used in NSM FRP strengthening of structures, including round, square, and rectangular bars [8]. As a special form of rectangular bars with a large cross-sectional height-to-thickness ratio, FRP strips are an attractive form of NSM FRP reinforcement due to their superior bond performance over NSM FRP bars of other shapes. This is because an FRP strip usually has a much larger perimeter for the same cross-sectional area than an FRP bar of other sectional shape and hence better bond performance, allowing a fuller utilization of the tensile strength of the FRP material [e.g. 12, 13]. Against this background, the present study is only concerned with NSM FRP strips which are defined as narrow rectangular FRP bars with a sectional height-to-thickness ratio not less than 5 [14]. For ease of presentation, the discussions in the paper are limited to simply supported beams.

In RC beams strengthened in flexure with NSM FRP bars, several debonding failure modes have been observed in laboratory tests, including end debonding failure and intermediate crack (IC) induced debonding failure. End cover separation (Fig. 1), as one of the end debonding failure modes, has been found to be by far the most common failure mode [8, 10].

The end cover separation failure process is initiated by the formation of a vertical crack in the un-strengthened region but near the critical end of the FRP reinforcement, followed by the propagation of a major crack at the level of the tension steel reinforcement towards the middle of the strengthened region. Another possible end debonding failure mode, namely interfacial debonding at the FRP-to-concrete interface, has been rarely if ever observed in laboratory tests [10] and is thus not covered in the present study. A major reason that end cover separation is much more likely than end interfacial debonding is the significant radial stresses generated by the steel tension bars on the surrounding concrete, making the plane of steel tension bars a more critical plane than the plane near the adhesive-concrete bi-material interface [15].

For RC beams strengthened with externally bonded FRP reinforcement, a large number of finite element studies on end cover separation failure have been undertaken [e.g. 16-18] and several strength models for this failure mode have been established [e.g. 19-22]. By contrast, for RC beams strengthened with NSM FRP reinforcement, very limited research has been conducted on finite element modelling [15, 23] or the establishment of strength models [24, 25] for the end cover separation failure mode. This situation is not surprising as the NSM FRP strengthening method emerged much later than the externally bonded FRP method and the associated research challenges are greater due to the presence of a large number of significant parameters.

To predict end cover separation failure in RC beams strengthened with NSM FRP reinforcement, a full 2-D (plane stress) nonlinear finite element (FE) approach (referred to as "the full FE approach" for brevity) has recently been developed by the authors [15, 23]. Using this full FE approach, the important factors that influence the accuracy of FE

prediction of end cover separation failure have been identified. One of the factors is the radial stresses exerted by the steel tension reinforcement onto the surrounding concrete, which was introduced by the authors into FE modelling of end cover separation failure in RC beams strengthened with FRP for the first time [15, 23]. Based on the findings from the full FE approach, a simplified 2-D (plane stress) FE approach (referred to as "the simplified FE approach" for brevity) [26, 27], in which only the part of the RC beam between the two adjacent cracks nearest to the critical end of the FRP reinforcement is included, was established for predicting end cover separation failure. This paper presents a study which was conducted using this simplified FE approach for the development of a debonding strength model for end cover separation failure in RC beams strengthened in flexure with NSM FRP strips.

2 Existing strength models

To date, only two strength models for end cover separation in RC beams strengthened in flexure with NSM FRP have been proposed [24, 25], and both of them are based on the concept of the so-called concrete tooth model (CTM) (Fig. 2). In a CTM, the "tooth" (Fig. 2), which is the concrete cover between two adjacent cracks, is treated as a cantilever, with the horizontal shear stress τ (from the NSM FRP) acting on its tip (i.e. free end). In addition to these two models, Hassan and Rizkalla [28] proposed a model based on interfacial stress analysis between NSM FRP strips and concrete to predict end interfacial debonding failure (another important end failure mode) in RC beams strengthened with NSM CFRP strips. For comparison purposes, Hassan and Rizkalla's model [28] is also introduced in this section although it deals with a slightly different failure mode.

116 *2.1 De Lorenzis and Nanni's model [24]*

117 Based on Zhang et al.'s model (the first CTM for end cover separation) [29] for RC beams
118 strengthened in flexure with an externally bonded steel plate, De Lorenzis and Nanni [24]
119 proposed a strength model for end cover separation in RC beams strengthened in flexure with
120 NSM FRP round bars. Assuming a linear elastic behaviour, the maximum tensile stress σ_A
121 at the root of the concrete tooth (Point A in Fig. 2) can be calculated as

122 $$\sigma_A = \frac{M_A}{I_A}\left(\frac{l}{2}\right) \tag{1}$$

123 where $M_A = \tau n \pi d_b l h'$ is the bending moment at the foot of the concrete tooth, $I_A = bl^3/12$
124 is the second moment of area of the concrete tooth cross-section, h' is the vertical distance
125 between the root of the concrete tooth and the centroid of the NSM FRP, b is the width of
126 the RC beam, d_b is the diameter of the FRP round bars, n is the number of FRP bars, τ
127 is the average interfacial shear stress between the NSM FRP bars and the concrete, and the
128 width of the concrete tooth l is either the minimum stabilized crack spacing, $l_{\min}$, or the
129 maximum stabilized crack spacing, $l_{\max} = 2l_{\min}$. The minimum stabilized crack spacing
130 $l_{\min}$ is given by

131 $$l_{\min} = \frac{A_e f_t}{u_s \sum O_{bars} + u_{NSM} \sum O_{NSM}} \tag{2}$$

132 where $f_t = 0.36\sqrt{f_{cu}}$ (both f_t and f_{cu} are in *MPa*) is the concrete tensile strength
133 while f_{cu} is the concrete cube compressive strength; $\sum O_{bars}$ is the sum of perimeters of all
134 the steel tension bars; $u_s = 0.28\sqrt{f_{cu}}$ (both u_s and f_{cu} are in *MPa*) is the average shear
135 bond strength between the steel bars and the concrete; $\sum O_{NSM}$ is the sum of perimeters of
136 all the NSM FRP round bars; u_{NSM} is the average shear bond strength between the NSM

FRP bars and the concrete; $A_c = 2h_1 b$ is the cross-sectional area of tensile concrete in a beam section, which is taken to be the product of twice the vertical distance between the centroid of tension steel and the soffit of beam (i.e. h_1) and the beam width. De Lorenzis and Nanni [24] recommended that u_{NSM} be taken as the local bond strength between NSM FRP bars and concrete.

Substituting M_A and I_A into Eq. 1 and assuming that cover separation failure occurs when the tensile stress σ_A is equal to the tensile strength of concrete f_t, the average interfacial shear stress $\tau_{failure}$ between FRP and concrete at cover separation failure can be found as

$$\tau_{failure} = \frac{f_t l}{6h'} \frac{b}{n\pi d_b} \tag{3}$$

The interfacial shear stress is balanced by the axial stress in the FRP. At the critical location (such as the loading point for three-point or four-point bending beams), the axial stress in the FRP at cover separation failure can be found as

$$\sigma_{failure} = \frac{4\tau_{\text{failure}} L_p}{d_b} = \frac{2lbf_t L_P}{3n\pi h' d_b^2} \tag{4}$$

by assuming that the interfacial stress is uniformly distributed over the effective length of the NSM bars L_p. De Lorenzis and Nanni (2003) proposed the following expressions to estimate the effective length L_p:

$$L_p = \min\,(L_{p1}, L_{p2}) \tag{5}$$

$$L_{p2} = 1.86 l_{\min}^2 - 127 l_{\min} + 2436 \qquad if \qquad l_{\min} \le 50mm \tag{6a}$$

$$L_{p2} = 736 \qquad if \qquad l_{\min} > 50mm \tag{6b}$$

where L_{p1} is the length of the NSM FRP bar in the shear span.

158

159 *2.2 Al-Mahmoud et al.'s model [25]*

160 Al-Mahmoud et al. [25] proposed a strength model of end cover separation in RC beams
161 strengthened with NSM FRP round bars. Their model is also based on the general concept of
162 the CTM, but the methodology is slightly different from that proposed by De Lorenzis and
163 Nanni [24].

164

165 Al-Mahmoud et al. [25] related the bending moment at the root of the concrete tooth to the
166 axial stress in the FRP bar at the left cracked section (i.e. the left vertical surface of the
167 concrete tooth in Fig. 2, which is referred to as the critical cracked section in this paper) as

168 $$M_A = \sigma_f A_f h' = \sigma_f n \pi d_b^2 h' \tag{7}$$

169 Combining Eqs. 1 and 7 and assuming that end cover separation occurs when the tensile
170 stress σ_A reaches the tensile strength of concrete f_t, the axial stress in the FRP bar at the
171 critical cracked section can be expressed as

172 $$\sigma_f = \frac{b_c l^2}{6\pi n d_b^2 h'} f_t \tag{8}$$

173 The axial stress in the FRP bar can be related to the bending moment M_l at the critical
174 cracked section of the strengthened beam as

175 $$\sigma_f = n_f \left(\frac{h_0 - y_0}{I_{cr}} \right) M_l \tag{9}$$

176 where $n_f = E_f / E_c$ is the elastic modulus ratio between FRP and concrete, I_{cr} is the
177 second moment of area of the cracked section transformed to concrete, h_0 is the vertical
178 distance between the compression face of the beam and the centroid of the NSM FRP
179 reinforcement, and y_0 is the vertical distance between the compression face of the beam and

the neutral axis of the critical cracked section. Combining Eqs. 8 and 9 leads to the following expression for the bending moment at the critical cracked section of the strengthened beam at cover separation failure:

$$M_l = \frac{f_t I_{cr} b l^2}{6 n_f n \pi d_b^2 h' (h_0 - y_0)} \tag{10}$$

2.3 Hassan and Rizkalla's model [28]

Hassan and Rizkalla [28] established a model for the end interfacial debonding strength of RC beams strengthened with CFRP strips. Based on the interfacial stress analysis by Malek et al. [30] of RC beams strengthened with an externally bonded FRP plate, Hassan and Rizkalla [28] proposed a closed-form solution for the interfacial shear stress τ between the NSM FRP strip and the concrete in RC beams strengthened with NSM FRP strips, which leads to the following two equations for a simply supported beam subjected to 3-point bending (Eq. 11) and 4-point bending (Eq. 12) respectively:

$$\tau = \frac{t_f}{2}\left[\frac{n_f P a y_{eff}}{2 I_{eff}} \omega e^{-\omega x} + \frac{n_f P y_{eff}}{2 I_{eff}}\right] \tag{11}$$

$$\tau = \frac{t_f}{2}\left[\frac{n_f P y_{eff}}{I_{eff}} + \frac{n_f P y_{eff} a}{I_{eff}} \omega e^{-\omega x}\right] \tag{12}$$

$$\omega^2 = \frac{2 G_a}{t_a t_f E_f} \tag{13}$$

where x is the horizontal distance from the critical end of the FRP strip; t_f is the thickness of the FRP strip; P is the concentrated load on the beam; y_{eff} is the vertical distance between the FRP strip centroid and the neutral axis of the beam section; I_{eff} is the effective second moment of area of the beam cross-section and can be calculated using Eq. 14;

201 e is the base of natural algorithm; G_a is the shear modulus of the adhesive; t_a is the
202 thickness of the adhesive layer; and a is the horizontal distance between the critical end of
203 the FRP strip and the nearest beam support.

204 $$I_{eff} = \left(\frac{M_{cr}}{M_{ap}}\right)^3 I_g + \left(1 - \left(\frac{M_{cr}}{M_{ap}}\right)^3\right) I_{cr} \quad (14)$$

205 where M_{cr} is the cracking moment of the beam section; M_{ap} is the bending moment
206 acting on a beam section; I_g is the gross second moment of area of the strengthened section
207 transformed to concrete; and I_{cr} is the second moment of area of the cracked section
208 transformed to concrete.
209
210 Obviously, the interfacial shear stresses calculated using Eqs. 11 and 12 achieve the largest
211 values when x is equal to zero (i.e. at the end of the FRP strip). By using the
212 Mohr-Coulomb failure criterion, the interfacial shear stress at the end of the FRP strip at
213 interfacial debonding failure, $\tau_{\max}$, can be determined from the following equation:

214 $$\tau_{\max} = \frac{f_c f_t}{f_c + f_t} \quad (15)$$

215 where f_c is the concrete cylinder compressive strength; and f_t is the concrete tensile
216 strength. Substituting Eq. 15 into Eq. 11 or Eq.12 with x=0 yields the applied load at
217 interfacial debonding failure of the FRP strip end.
218
219 *2.4 Summary*
220 As can be seen from the above review, in the end cover separation strength model proposed
221 by Al-Mahmoud et al. [25] and the end interfacial debonding strength model proposed by
222 Hassan and Rizkalla [28], the concrete is assumed to be a linear elastic material in

compression; in De Lorenzis and Nanni's model [24], the concept of effective length of the NSM FRP is introduced, and in the effective length region, the interfacial stress is assumed to be uniformly distributed. In all three models, the bonded interface between FRP and concrete and that between steel bars and concrete are assumed to experience no interfacial slips. Despite these assumptions, which may lead to significant prediction errors, they represent valuable attempts at formulating strength models for end debonding failures in RC beams strengthened with NSM FRP reinforcement.

In the present study, only Al-Mahmoud et al.'s model [25] and Hassan and Rizkalla's model [28] are compared with the present model. De Lorenzis and Nanni's model [24] was developed for NSM FRP round bars and cannot be easily adapted for use of NSM FRP strips. Although Al-Mahmoud et al.'s model [25] was originally proposed for RC beams strengthened with NSM round FRP bars, it can be easily modified for application to RC beams strengthened with NSM FRP strips: by replacing the formula for cross-sectional area for a circular section with that for a rectangular section.

When comparing Hassan and Rizkalla's model [28] with the present model in predicting end cover separation failure, it should be noted that the former is for end interfacial debonding while the latter is for end cover separation. However, it can be expected that the failure load predicted by Hassan and Rizkalla's model [28] should not be smaller than the test result as well as the prediction from the present model; otherwise, the beam should have failed by end interfacial debonding instead of end cover separation. The comparison thus can be used to check whether Hassan and Rizkalla's model [28] does provide an upper bound prediction.

3 Simplified FE approach for end cover separation

The simplified FE model developed by Zhang and Teng [26, 27] for cover separation failure in FRP-strengthened RC beams was employed in a parametric study to generate numerical data for use in the formulation of a strength model. A brief summary of this simplified FE model is given herein to set the background for the parametric study. For more details of this simplified FE model, the reader is referred to Ref. [27].

In the simplified FE model, the segment of the RC beam between the two major cracks near the critical end of the FRP reinforcement is isolated to form the model for analysis (Fig. 3), with the moments acting on the two cracked sections being imposed using two pairs of external loads (R and P_3 as one pair on the critical, left cracked section, and P_1 and P_2 as another pair on the other cracked section at the FRP strip end in Fig. 3). A rigid plate is attached to each cracked section to enforce the plane section assumption. As can be seen from Fig. 3, if the strain in the FRP reinforcement at the critical crack (Point B in Fig. 3) at end cover separation is known, the moment acting on the same section can be obtained through section analysis. The concrete is modelled using 4-node plane stress elements; the steel reinforcement is simulated using 2-node beam elements and both sides of the steel reinforcement are connected to the rigid plates. The cohesive-element-pair (CEP) proposed by Zhang and Teng [26, 27] is used to simulate the radial stresses exerted by the tension steel bars onto the surrounding concrete when they are in tension. The FRP is modelled using 2-node beam elements located at the centroid of the NSM FRP reinforcement. Only one end (the left end in Fig. 3) of the FRP reinforcement is connected to the adjacent rigid plate, while the other end (the right end) representing the actual end of the FRP reinforcement and is left free.

The behaviour of cracked concrete is simulated using the orthogonal fixed smeared crack model. The crack band concept [31] is employed in the simplified FE model with the fracture energy being that given by CEB-FIP [32]. The maximum tensile stress criterion is adopted to describe the initiation of cracking while the yield surface proposed by Buyukozturk [33] with the associated flow rule is used to describe the compression-dominated behaviour of concrete. The tension-softening behaviour and the shear stress-slip behaviour of cracked concrete as well as the compressive behaviour of concrete are properly modelled. The FRP is modelled as an elastic isotropic brittle material, and the steel reinforcement including tension bars, compression bars and stirrups is modelled as an elastic-perfectly plastic material. The interfacial behaviour between longitudinal steel bars and concrete is simulated using the bond-slip model given in CEB-FIP [29] while that between NSM FRP strips and concrete is simulated using the bond-slip model proposed by Zhang et al. [34]. The latter means that the FE model is only applicable to RC beams strengthened in flexure with NSM CFRP strips although applicability to other forms of FRP reinforcement can be easily enabled by replacing Zhang et al.'s bond-slip model [34] with an appropriate model.

4 Strength model for end cover separation

As explained earlier, if the strain in the FRP reinforcement at the critical cracked section (Point B in Fig. 3) at end cover separation failure (i.e. the debonding strain in the FRP or simply the debonding strain) can be obtained, a section analysis can be conducted to find the moment acting on the critical cracked section based on the plane section assumption, and the shear force and the load level of the beam can be easily found from the bending moment value for a given load distribution. The proposed debonding strength model for end cover separation failure thus consists of a method for predicting debonding strain and a conventional section analysis based on the plane section assumption, with the former being

297 the key element. In the present study, the section analysis is based on the BS 8110 [35]
298 compressive stress-strain curve of concrete, so the ultimate concrete compressive strain is
299 taken to be 0.0035.
300
301 *4.1 Debonding strain in the FRP at end cover separation*
302 The FE approach described earlier was used to conduct a parametric study to generate
303 numerical results for the development of an approximate equation for the debonding strain.
304 The following geometric and material properties define the reference case for the parametric
305 study unless otherwise specified: concrete cylinder compressive strength f_c =30 *MPa*; elastic
306 modulus of FRP E_f =150 *GPa*; cross-sectional area of FRP strip A_f = 40 mm^2; thickness of
307 FRP strip = 2 *mm*; second moment of area of FRP strip I_f = 1333 mm^4; vertical distance
308 between the centroids of the steel and the FRP reinforcements c_d = 30 *mm*; crack spacing s_c
309 = 100 *mm* (length of the beam segment in the FE model); height of the beam h = 300 *mm*;
310 width of the beam b = 150 *mm*; sum of diameters of all steel tensions bars D_t = 24 *mm* (i.e.
311 $2\phi 12$); and moment ratio between the right and the left cracked beam sections of the concrete
312 tooth β_P =0.5.
313
314 *4.1.1 Effect of second moment of area of FRP strip*
315 The second moment of area of the FRP strip, I_f , was varied from 1×10^3 mm^4 to
316 2×10^4 mm^4 to examine its effect on the debonding strain. The cross-sectional area of the FRP
317 strip was kept constant at 40 mm^2 , but the height and thickness of the FRP strip
318 cross-section were changed to achieve the desired I_f value. Note that for the reference
319 beam with a width of 150 mm, $I_f = 5\times10^3$ mm^4 , which is a practically likely value (e.g.

320 I_f = 5.2×10^3 mm^4 for two 2×25 mm NSM CFRP strips). Therefore, the selected range of

321 I_f values was large enough to cover practical situations and to examine its influence.

322

323 The predicted debonding strains are listed in Table 1. The maximum difference between the

324 predicted FRP strains is only about 2% within the range of I_f values investigated, so it

325 may be concluded that for practical applications, the effect of I_f is minimal and can be

326 neglected.

327

328 *4.1.2 Effect of beam height*

329 Table 2 provides the predicted debonding strains for three beam heights: h = 300 *mm*, 600

330 *mm*, and 900 *mm*; all other properties are the same as those of the reference case. Clearly

331 the effect of beam height is also insignificant, so it can also be neglected in evaluating the

332 debonding strain in the FRP.

333

334 *4.1.3 Effect of moment ratio*

335 The effect of moment ratio β_P was examined for three different concrete strengths (f_c = 20

336 *MPa*, 30 *MPa* and 40 *MPa*), four values of the distance between the steel and the FRP

337 reinforcements (c_d =15 *mm*, 30 *mm*, 45 *mm*, and 60 *mm*), and four different crack spacings

338 (s_c = 50 *mm*, 75 *mm*, 100 *mm*, and 150 *mm*). In each case, the moment ratio between the right

339 and the left cracked beam sections of the concrete tooth was varied from 0 to 1.0 at an

340 interval of 0.1. The predicted debonding strains, normalized with respect to the debonding

341 strain of the corresponding case with a moment ratio of 0.6, are shown in Fig. 4. For ease of

342 reference, each numerical case (or numerical specimen) in Fig. 4 is given a name, which

343 starts with a number to represent the cylinder compressive strength of concrete (f_c),

followed by a number to represent the elastic modulus of FRP (E_f), and then a number to represent the distance between steel and FRP reinforcements (c_d), and finally a number to represent the crack spacing (s_c). It is seen that as the moment ratio increases, the debonding strain first increases nearly linearly regardless of the values of the other parameters (i.e. f_c, c_d and s_c) until the moment ratio reaches 0.6; afterwards, the debonding strain decreases nearly linearly. All of the normalized curves shown in Fig. 4 are almost identical to each other, with most values falling in the range from 0.9 to 1. The effect of moment ratio on the debonding strain is therefore small and is ignored in the approximate predictive equation for debonding strain presented later in the paper.

4.1.4 Effect of axial rigidity of FRP strip

The axial rigidity of the FRP strip $A_f E_f$ was varied from 2000 *kN* ($20\,mm^2 \times 100\,GPa$) to 16000 *kN* ($80\,mm^2 \times 200\,GPa$) to study its effect on the debonding strain. The relationship between the FRP debonding strain obtained from FE analysis and the reciprocal of FRP axial rigidity $A_f E_f$ is plotted in Fig. 5, from which it can be seen that the variation of the FE debonding strain with the reciprocal of FRP strip axial rigidity follows approximately a power function.

4.1.5 Effect of concrete strength

The effect of concrete strength f_c was examined for three different values of the elastic modulus of FRP (E_f = 100 *GPa*, 150 *GPa*, and 200 *GPa*) and four different values of the cross-sectional area of FRP strip (A_f = 20 mm^2, 40 mm^2, 60 $mm^2$and 80 mm^2). The other geometric and material properties of the beams were the same as those of the reference beam.

The predicted relationship between the debonding strain and the concrete strength is shown in Fig. 6, which indicates that the FRP strain is approximately proportional to $\sqrt{f_c}$. Each numerical specimen in Fig. 6 is given a name, which starts with a number to represent the elastic modulus of FRP (E_f) and is then followed by a number to represent the cross-sectional area of FRP strip (A_f).

4.1.6 Effects of crack spacing and distance between steel and FRP reinforcements

The effect of distance between steel reinforcement and FRP reinforcements, c_d, was examined by obtaining FE predictions for four different values: 15 *mm*, 30 *mm*, 45 *mm*, and 60 *mm*. The effect of crack spacing, s_c, was also examined by obtaining FE predictions for four different values: 50 *mm*, 75 *mm*, 100 *mm*, and 150 *mm*. The relationship between the debonding strain and c_d is shown in Fig. 7 while that between the debonding strain and s_c is shown in Fig. 8. Fig. 7 indicates that the debonding strain decreases nearly linearly as the value of c_d increases, with the slopes of the linear best-fit lines for different s_c values being nearly the same. Fig. 8 indicates that the debonding strain increases with the value of s_c. As the value of c_d increases, the relationship between the debonding strain and s_c changes from a power function to a linear function. To see a clearer trend, the debonding strains normalized with respect to the strain of the case with a c_d value of 30 mm are shown in Fig. 9, which indicates that the normalized strain decreases nearly linearly as the value of c_d increases regardless of the values of s_c and the magnitude of slope of the linear best-fit lines decreases as the value of s_c increases.

389 *4.1.7 Effects of beam width and sum of steel tension bar diameters*

390 The debonding strain in the FRP is expected to be proportional to the clear width of the beam

391 $b_{clear} = b - D_t$, where D_t is the sum of diameters of all the steel tension bars (or more

392 precisely all the steel tension bars of the lowest row if multiple rows of steel tension bars are

393 used), if other parameters are the same. Furthermore, the debonding strain is expected to

394 depend on the b_{clear}/D_t ratio as the effect of radial stresses from steel tension bars is affected

395 by the b_{clear}/D_t ratio. In the parametric study, the following beam widths were examined: 50

396 *mm*, 100 *mm*, 150 *mm*, 200 *mm*, and 250 *mm*, with the corresponding b_{clear}/D_t ratios being

397 1.08, 3.17, 5.25, 7.33 and 9.42. The corresponding values chosen for the cross-sectional area

398 of the FRP strip, A_f, are 8.25 mm^2, 24.13 mm^2, 40.00 mm^2, 55.88 mm^2 and 71.75 mm^2, in

399 order to keep the A_f/b_{clear} ratio constant. Fig. 10 shows that the predicted debonding strain

400 increases with the b_{clear}/D_t ratio approximately following a power function.

401

402 *4.1.8 Approximate equation for the debonding strain*

403 Based on the regression analysis of the results of 168 numerical specimens examined in the

404 parametric study, Eq. 16 is proposed as a design model for predicting the debonding strain in

405 the FRP at end cover separation failure:

406 $$\varepsilon_{db} = 10^4 \times \beta_{cs}\beta_{AE}\beta_{bod}b_{clear}\sqrt{f_c} \quad (16)$$

407 $$\beta_{cs} = \left(\frac{4.5}{s_c^{0.3}} - \frac{c}{s_c}\right)\left(\frac{s_c}{100} - 0.1\right) \quad (17)$$

408 $$\beta_{AE} = \frac{1}{\left(A_f E_f\right)^{0.9}} \quad (18)$$

409 $$\beta_{bod} = \left(\frac{b_{clear}}{D_t} \right)^{0.1} \quad (19)$$

410 where β_{cs} reflects the combined effect of c_d (distance between the steel and the FRP
411 reinforcements, in *mm*) and s_c (crack spacing, in *mm*); β_{AE} reflects the effect of axial
412 rigidity of FRP strip $A_f E_f$ (A_f in mm^2 and E_f in *GPa*); and β_{bod} reflects the effect of
413 ratio between beam clear width b_{clear} (in *mm*) and sum of steel tension bar diameters D_t
414 (in *mm*). The concrete cylinder strength f_c is in *MPa*.

415

416 A comparison between the predictions of the simplified FE model and the debonding strain
417 equation (Eq. 16) is shown in Fig. 11, indicating very close agreement between the two sets
418 of results. The ratios between the predictions of Eq. 16 and the FE predictions have an
419 average value of 1.00 and a coefficient of variation (CoV) of 0.070.

420

421 *4.2 Crack spacing*

422 To determine the debonding strain as well as the distance between the left cracked section
423 and the nearest support, the crack spacing is needed as input. In the present study, the
424 minimum stabilized crack spacing, $s_c^{\min}$, proposed by Zhang et al. [29] is adopted:

425 $$s_c^{\min} = \frac{A_e f_t}{u_s \sum O_{bars} + u_f C_{failure}} \quad (21)$$

426 where $u_f = 0.28\sqrt{f_{cu}}$ is the average shear bond strength between FRP and concrete, $C_{failure}$
427 is the perimeter length of the failure plane which is taken to be the total length of the three
428 groove sides. In the next section, the minimum stabilized crack spacing, $s_c^{\min}$, the maximum
429 stabilized crack spacing, $2s_c^{\min}$, and an intermediate value, $1.5s_c^{\min}$, are all examined to

investigate the effect of crack spacing.

5 Comparison with test data

For the proposed debonding strain equation for end cover separation to be used with confidence in practical design, its accuracy needs to be assessed using laboratory test data. The test data of 10 RC beams strengthened with NSM FRP strips were collected from the published literature for this purpose. For all these 10 beams, sufficient details have been provided in the papers for them to be used in the comparison. Details of these 10 test beams are given in Tables 3 and 4. In addition to the present debonding strength model, the models of Al-Mahmoud et al. [25] and Hassan and Rizkalla [28] are also included in the comparison.

The predictions of the present debonding strength model for three different crack spacings (i.e. $s_c = s_c^{\min}$, $1.5s_c^{\min}$ and $2s_c^{\min}$ respectively) are compared in Fig. 12 with the test results. The predictions of the two existing models for these 10 RC beams are compared with the test results in Figs. 13 and 14 respectively. All the predictions and the test results for the shear force are listed in Tables 5.

The proposed strength model with a crack spacing of $1.5s_c^{\min}$ leads to an average prediction-to-test ratio of 1.10 and a CoV of 0.108 (Table 5). These statistical indicators are better than those for predictions of the proposed strength model obtained with crack spacings of $s_c^{\min}$ and $2s_c^{\min}$, for which the average prediction-to-test ratios are 0.863 and 1.17, and the CoVs are 0.180, 0.147 respectively. Nevertheless, the proposed strength model with any of the three crack spacing values offers much closer predictions of the test results than the two existing models proposed by Al-Mahmoud et al. [25] and Hassan and Rizkalla [28]

454 respectively. The predictions from Hassan and Rizkalla's model [28] are very conservative
455 with a large scatter, with the prediction-to-test average ratio and CoV being 0.555 and 0.467
456 respectively, indicating that Hassan and Rizkalla's model [28] fails to provide a reasonable
457 upper bound prediction. The predictions of Al-Mahmoud et al.'s model [25], on the contrary,
458 are very un-conservative with an even larger scatter, with the average prediction-to-test ratio
459 and CoV being 1.90 and 0.702 respectively. The superior performance of the proposed
460 debonding strength model is also clearly demonstrated by the comparisons given in Figs. 12
461 to 14.
462

463 ## 6 Concluding remarks

464 This paper has been concerned with the development of a strength model for predicting the
465 end cover separation failure load of RC beams strengthened with FRP strips (i.e. rectangular
466 FRP bars with a sectional height-to-thickness ratio not less than 5). The approach taken was
467 to develop an approximate equation for the debonding strain in the FRP strips at the critical
468 cracked section at end cover separation failure (i.e. the debonding strain) and to find the
469 moment acting in the critical cracked section by conventional section analysis based on the
470 plane section assumption (i.e. the debonding moment). Once the debonding moment is
471 known, the associated shear force and the load level at cover separation failure can be easily
472 determined for any given load distribution. The debonding strain equation is thus the key
473 element of the proposed debonding strength model. In practice, the alternative approach of
474 checking the strain in the FRP strips at the critical cracked section against the prediction of
475 the proposed debonding strain equation can be adopted to design again cover separation
476 failure.
477

478 To formulate an approximate equation for the debonding strain, an efficient FE approach

recently proposed by the authors [26, 27] was employed in a parametric study to obtain extensive numerical results. These results were presented and examined to understand how each parameter affects this debonding strain, based on which an appropriate equation for the debonding strain was proposed. The proposed strength model as well as with two existing strength models for end debonding failure was compared with a test database assembled from the published literature. These comparisons showed that the proposed strength model leads to predictions in close agreement with the test results and is far more accurate than the two existing models.

Acknowledgement

The authors are grateful for the financial support received from the National Basic Research Program of China ("973" Program) (Project No.: 2012CB026201) and the Research Grants Council of the Hong Kong Special Administrative Region (Project Nos: PolyU 5315/09E).

References

[1] Teng, J. G., Chen, J. F., Smith, S. T., and Lam, L. (2002). *FRP-strengthened RC Structures*, West Sussex: Wiley.

[2] Oehlers, D. J. and Seracino, R. (2004). *Design of FRP and steel plated RC structures: retrofitting beams and slabs for strength, stiffness and ductility*. Elsevier.

[3] Bank L.C. (2006). *Composites for construction: Structural design with FRP materials.* West Sussex: Wiley, UK.

[4] Yao, J. and Teng, J. G. (2007). "Plate end debonding in FRP-plated RC beams - I: Experiments." *Engineering Structures*, 29(10), 2457-2471.

[5] Hollaway, L. C. and Teng, J. G., eds. (2008). *Strengthening and rehabilitation of civil*

infrastructures using FRP composites, Woodhead, Cambridge, U.K.

[6] Barros, J. A. O., Dias, S. J. E., and Lima, J. L. T. (2007). "Efficacy of CFRP-based techniques for the flexural and shear strengthening of concrete beams." *Cement & Concrete Composites*, 29(3), 203-217.

[7] Barros, J. A. O., Varma, R. K., Sena-Cruz, J. M., and Azevedo, A. F. M. (2008). "Near surface mounted CFRP strips for the flexural strengthening of RC columns: Experimental and numerical research." *Engineering Structures*, 30(12), 3412-3425.

[8] De Lorenzis, L. and Teng, J. G. (2007). "Near-surface mounted FRP reinforcement: an emerging technique for strengthening structures." *Composites: Part B*, 38(2), 119-143.

[9] Soliman, S.M., El-Salakawy, E. and Benmokrane, B. (2011). "Bond performance of near-surface-mounted FRP bars." *Journal of Composites for Construction, ASCE*, 15(1), 103-111.

[10] Zhang, S. S. (2012). *Behaviour and modelling of RC beams strengthened in flexure with near-surface mounted FRP strips*. PhD thesis, The Hong Kong Polytechnic University, Hong Kong, China.

[11] Peng, H., Zhang, J. R., Cai, C. S, Liu, Y. (2014). "An experimental study on reinforced concrete beams strengthened with prestressed near surface mounted CFRP strips." *Engineering Structures*, 79, 222-233.

[12] El Hacha, R. and Rizkalla, S.H. (2004). "Near-surface-mounted fiber-reinforced polymer reinforcements for flexural strengthening of concrete structures." *ACI Structural Journal*, 101(5), 717-726.

[13] Perera, W.K.K.G., Ibell, T.J. and Darby, A. P. (2009). "Bond behaviour and effectiveness of various shapes of NSM CFRP bars." *Proceedings, 9th International Symposium on Fiber-Reinforced Polymers Reinforcement for Concrete Structures (FRPRCS-9)*, 13-15 July, Sydney, Australia (CD-ROM).

[14] Zhang, S. S., Teng, J. G. and Yu, T. (2014). "Bond strength model for CFRP strips near-surface mounted to concrete." *Journal of Composites for Construction, ASCE*, 18, SPECIAL ISSUE: 10th Anniversary of IIFC, A4014003.

[15] Zhang, S.S. and Teng, J.G. (2014). "Finite element analysis of end cover separation in RC beams strengthened in flexure with FRP", *Engineering Structures*, 75, 550-560.

[16] Arduini, M., Tommaso, A. D., and Nanni, A. (1997). "Brittle failure in FRP plate and sheet bonded beams." *ACI Structural Journal* 94(4), 363-370.

[17] Rahimi, H. and Hutchinson, A. (2001). "Concrete beams strengthened with externally bonded FRP plates." *Journal of Composites for Construction, ASCE*, 5(1), 44-56.

[18] Pham, H.B. and Al-Mahaidi, R. (2005) "Finite element modelling of RC beams retrofitted with CFRP fabrics." *Proceedings, 7th International Symposium on Fiber Reinforced Polymer Reinforcement for Reinforced Concrete Structures*, American Concrete Institute 2005, SP-230, 499-514.

[19] Oehlers, D. J. (1992). "Reinforced-concrete beams with plates glued to their soffits." *Journal of Structural Engineering, ASCE*, 118(8), 2023-2038.

[20] Oehlers, D. J., Liu, I. S. T., Seracino, R. and Ali, M. S. M. (2004). "Prestress model for shear deformation debonding of FRP- and steel-plated RC beams." *Magazine of Concrete Research*, 56(8), 475-486.

[21] Gao, B., Leung, C. K. Y. and Kim, J. K. (2005). "Prediction of concrete cover separation failure for RC beams strengthened with CFRP strips." *Engineering Structures*, 27(2), 177-189.

[22] Teng, J. G. and Yao, J. (2007). "Plate end debonding in FRP-plated RC beams-II: strength model." *Engineering Structures*, 29(10), 2472-2486.

[23] Zhang, S. S. and Teng, J. G. (2010). "Finite element prediction of plate-end cover separation in FRP-strengthened RC beams." *Proceedings, 11th International*

553 *Symposium on Structural Engineering*, December 18-20, 2010, Guangzhou, China, pp.
554 1794-1799.
555 [24] De Lorenzis, L. and Nanni, A. (2003). "Proposed design procedure of NSM FRP
556 reinforcement for strengthening of RC beams." *Proceedings, 6th International*
557 *Symposium on FRP Reinforcement for Concrete Structures*, July 8-10, 2003, Singapore,
558 pp. 1455-1464.
559 [25] Al-Mahmoud, F., Castel, A., Francois, R., and Tourneur, C. (2010). "RC beams
560 strengthened with NSM CFRP rods and modeling of peeling-off failure." *Composite*
561 *Structures*, 92(8), 1920-1930.
562 [26] Zhang, S.S. and Teng, J.G. (2013). "Simplified finite element modelling of end cover
563 separation in RC beams flexurally-strengthened with bonded FRP reinforcement."
564 *Proceedings, 4th Asia Pacific Conference on FRP Composites in Structures (APFIS)*,
565 December, 11-13, 2013, Melbourne, Australia. (CD-ROM).
566 [27] Zhang, S.S. and Teng, J.G. (2015). "End cover separation in RC beams strengthened in
567 flexure with bonded FRP reinforcement: simplified finite element approach." Materials
568 and Structures, in press. DOI: 10.1617/s11527-015-0645-z.
569 [28] Hassan, T. K. and Rizkalla, S. H. (2003). "Investigation of bond in concrete structures
570 strengthened with near surface mounted carbon fiber reinforced polymer strips."
571 *Journal of Composites for Construction, ASCE*, 7(3), 248-257.
572 [29] Zhang, S., Raoof, M. and Wood, L. A. (1995). "Prediction of peeling failure of
573 reinforced-concrete beams with externally bonded steel plates." *Proceedings, the*
574 *Institution of Civil Engineers-Structures and Buildings*, 110(3), 257-268.
575 [30] Malek, A. M., Saadatmanesh, H. and Ehsani, M. R. (1998). "Prediction of failure load
576 of R/C beams strengthened with FRP plate due to stress concentration at the plate end."
577 *ACI Structural Journal*, 95(1), 142-152.

578 [31] Bazant, Z.P. and Oh, B.H. (1983). “Crack band theory for fracture of concrete.”
579 *Materials and Structures*, 16(93), 155-177.
580 [32] CEB-FIP. (1993). *Model Code 90*, Lausanne, Switzerland.
581 [33] Buyukozturk, O. (1997). “Nonlinear analysis of reinforced concrete structures.”
582 *Computers and Structures* , 7, 149-156.
583 [34] Zhang, S.S., Teng, J.G. and Yu, T. (2013). “Bond-slip model for CFRP strips
584 near-surface mounted to concrete.” *Engineering Structures*, 56, 945–953.
585 [35] BS 8110. (1997). *Structural use of concrete-part 1: Code of practice for design and*
586 *construction*, London: British Standards Institute, UK.
587 [36] Barros, J. A. O. and Fortes, A. S. (2005). “Flexural strengthening of concrete beams
588 with CFRP laminates bonded into slits.” *Cement & Concrete Composites*, 27(4),
589 471-480.
590 [37] Teng, J. G., De Lorenzis, L., Wang, B., Rong, L., Wong, T. N. and Lam, L. (2006).
591 “Debonding failures of RC beams strengthened with near-surface mounted CFRP strips.”
592 *Journal of Composites for Construction, ASCE*, 10(2), 92-105.
593 [38] Thorenfeldt, E. (2007). “Bond capacity of CFRP strips glued to concrete in sawn slits.”
594 *Proceedings, 8th International Conference on Fibre Reinforced Plastics for Reinforced*
595 *Concrete Structures*, July 16-18, 2007, Patras, Greece (CD-ROM).

596

Notation

a = horizontal distance between critical end of FRP strip and nearest beam support

A_e = cross-sectional area of tensile concrete in a beam section

A_f = cross-sectional area of FRP strip

b = width of beam

b_{clear} = clear width of beam

c_d = vertical distance between centroids of steel and FRP reinforcements

d_b = diameter of FRP round bar

D_t = sum of diameters of all steel tension bars

e = base of natural algorithm

E_f = elastic modulus of FRP

f_t = concrete tensile strength

f_{cu} = concrete cube compressive strength

f_c = concrete cylinder compressive strength

G_a = shear modulus of adhesive

h = height of beam

h_0 = distance between compression face of beam and centroid of NSM FRP reinforcement

h_1 = vertical distance between centroid of tension steel and soffit of beam

h' = vertical distance between root of concrete tooth and centroid of NSM FRP reinforcement

L_p = effective length of NSM bar

L_{p1} = length of NSM FRP bar in shear span

I_A = second moment of area of concrete tooth cross-section

I_{cr} = second moment of area of cracked section transformed into concrete

I_{eff} = effective second moment of area of beam cross-section

I_f = second moment of area of FRP strip

I_g = gross second moment of area of strengthened beam section transformed to concrete

l = width of concrete tooth

$l_{\min}$, $l_{\max}$ = minimum stabilized crack spacing and maximum stabilized crack spacing used in De Lorenzis and Nanni's model

M_{ap} = bending moment at a beam section

M_A = bending moment at foot of concrete tooth

M_{cr} = cracking moment of beam section

M_l = bending moment at critical cracked section of strengthened beam

n = number of FRP bars

n_f = FRP-to-concrete elastic modulus ratio

P = concentrated load on beam

s_c, $s_c^{\min}$ = crack spacing; minimum stabilized crack spacing

t_a = thickness of adhesive layer

t_f = thickness of FRP strip

x = horizontal distance from critical end of FRP strip

y_0 = vertical distance between compression face of beam and neutral axis of critical cracked section

y_{eff} = vertical distance between FRP strip centroid and neutral axis of beam section

σ_A = maximum tensile stress at root of concrete tooth (Point A in Fig. 2)

$\sigma_{failure}$ = axial stress in FRP strip at cover separation failure

τ = interfacial shear stress between FRP and concrete

$\tau_{failure}$ = average interfacial shear stress between FRP and concrete at cover separation failure

$\tau_{\max}$ = interfacial shear stress at FRP strip end at interfacial debonding failure

u_s = average shear bond strength between steel bars and concrete

u_{NSM} = average shear bond strength between NSM FRP bars and concrete

$\sum O_{bars}$ = sum of perimeters of all steel tension bars

$\sum O_{NSM}$ = sum of perimeters of all NSM FRP round bars

β_P = moment ratio between right and left cracked beam sections of concrete tooth

Tables

Table 1. Effect of second moment of area of FRP bar on debonding strain

Second moment of area of FRP bar I_f (mm^4)	Debonding strain ε_{db} ($\mu\varepsilon$)	Percentage reduction
1×10^3	2483	0.00%
5×10^3	2472	0.44%
1×10^4	2455	1.13%
2×10^4	2435	1.93%

Table 2. Effect of beam height on debonding strain

Beam height h (mm)	Debonding strain ε_{db} ($\mu\varepsilon$)	Percentage reduction
300	2482	0.00%
600	2453	1.17%
900	2416	2.66%

Table 3. Details of RC beams strengthened with NSM FRP

Source	Specimen	b (mm)	h (mm)	h_0 (mm)	a (mm)	a_v (mm)	L (mm)	f_c (MPa)	E_c (GPa)
Ref. [36]	V2R2	100	177	157	50	500	1500	46.1	32.1
	V3R2	100	175	155	50	500	1500	46.1	32.1
	V4R3	100	180	160	50	500	1500	46.1	32.1
Ref. [37]	B500	150	300	256	1200	1200	3000	35.2	28.1
	B1200	150	300	256	900	1200	3000	35.2	28.1
	B1800	150	300	256	600	1200	3000	35.2	28.1
Ref. [6]	S2	120	170	146	60	300	900	52.2	34.2
	S3	120	170	146	60	300	900	52.2	34.2
Ref. [38]	B2	150	250	206	100	950	2500	50.0	33.4
	B5	150	250	206	100	950	2500	50.0	33.4

Note: b = width of beam; h = height of beam; h_0 = effective depth of beam; a = distance from a bar end to the nearest support; a_v = shear span of beam; L = span of beam; f_c = cylinder compressive strength of concrete; and E_c = elastic modulus of concrete.

Table 4. Details of steel bars and FRP strips for the test beams

Source	Specimen	E_f (GPa)	f_f (MPa)	t_f (mm)	h_f (mm)	E_s^{ten} (GPa)	f_y^{ten} (GPa)	A_s^{ten} (mm^2)	$(n/\phi)_{ten}$	E_s^{com} (GPa)	f_y^{com} (GPa)	A_s^{com} (mm^2)	$(n/\phi)_{com}$	E_{vc} (GPa)	f_{vy} (GPa)	A_{vc} (mm^2)	s_v (mm)
Ref. [36]	V2R2	158.8	2739.5	2.9	9.59	200	730	84.8	3/6	200	730	101	2/8	200	730	56.5	100
	V3R2	158.8	2739.5	2.9	9.59	200	730	107	2/6+1/8	200	730	101	2/8	200	730	56.5	100
	V4R3	158.8	2739.5	4.35	9.59	200	730	151	3/6	200	730	101	2/8	200	730	56.5	100
Ref. [37]	B500	151	2068	4	16	210	532	226	2/12	210	375	101	2/8	210	375	101	100
	B1200	151	2068	4	16.	210	532	226	2/12	210	375	101	2/8	210	375	101	100
	B1800	151	2068	4	16	210	532	226	2/12	210	375	101	2/8	210	375	101	100
Ref. [6]	S2	158.8	2740	2.8	9.6	200	627	66.4	2/6.5	200	627	66.4	2/6.5	200	540	56.5	80
	S3	158.8	2740	4.2	9.6	200	627	99.5	3/6.5	200	627	66.4	2/6.5	200	540	56.5	80
Ref. [38]	B2	157	2580	6	15	203	530	226	2/12	203	530	226	2/12	200	530	101	100
	B5	153	2500	5	20	203	530	226	2/12	203	530	226	2/12	200	530	101	100

Note: E_f = elastic modulus of FRP; f_f = tensile strength of FRP; t_f = thickness of FRP strip; h_f = height of FRP strip; E_s^{ten} = elastic modulus of steel tension bars; f_y^{ten} = yield stress of steel tension bars; A_s^{ten} = total cross-sectional area of steel tension bars; $(n/\phi)_{ten}$ = number/diameter of tension steel bars; E_s^{com} = elastic modulus of steel compression bars; f_y^{com} = yield stress of steel compression bars; A_s^{com} = total cross-sectional area of steel compression bars; $(n/\phi)_{com}$ = number/diameter of steel compression bars; E_{vc} = elastic modulus of stirrups; f_{vy} = yield stress of stirrups; A_{vc} = total cross-sectional area of stirrups; s_v = spacing of stirrups.

Table 5. Test and predicted ultimate shear forces for beams strengthened with NSM FRP

Source	Specimens	V_{test} (kN)	$V_{pre,1}$ (kN)	$\frac{V_{pre,1}}{V_{test}}$	$V_{pre,1.5}$ (kN)	$\frac{V_{pre,1.5}}{V_{test}}$	$V_{pre,2}$ (kN)	$\frac{V_{pre,2}}{V_{test}}$	V_{H-R} (kN)	$\frac{V_{H-R}}{V_{test}}$	V_{AI} (kN)	$\frac{V_{AI}}{V_{test}}$
Ref. [36]	V2R2	39.25	40.7	1.04	50.3	1.28	55.3	1.41	34.7	0.884	143	3.64
	V3R2	40.95	43.2	1.05	54.4	1.33	60.4	1.48	36.2	0.885	166	4.04
	V4R3	47.45	36.1	0.761	49.5	1.04	57.5	1.21	33.6	0.708	160	3.35
Ref. [37]	B500	23.9	17.0	0.710	24.7	1.03	25.4	1.06	5.10	0.213	15.1	0.631
	B1200	31.55	21.9	0.694	31.4	0.995	32.0	1.01	6.70	0.214	19.6	0.622
	B1800	45.85	30.9	0.673	43.2	0.942	43.1	0.940	10.0	0.218	28.2	0.614
Ref. [6]	S2	46.65	52.2	1.12	49.7	1.07	45.5	0.976	30.3	0.649	97.2	2.08
	S3	48.3	42.3	0.877	51.4	1.07	56.0	1.16	27.8	0.576	94.1	1.95
Ref. [38]	B2	63.9	59.1	0.925	74.9	1.17	83.3	1.30	36.4	0.542	69.9	1.04
	B5	65.5	51.4	0.785	67.5	1.03	76.5	1.17	41.5	0.610	66.2	0.973
Statistical indicators	**Average =**			0.863		1.10		1.17		0.555		1.90
	STD =			0.155		0.119		0.172		0.259		1.34
	CoV =			0.180		0.108		0.147		0.467		0.702

Note: $V_{pre,1}$ = shear force predicted by the proposed model with $s_c^{\min}$;

$V_{pre,1.5}$ = shear force predicted by the proposed model with $1.5s_c^{\min}$;

$V_{pre,2}$ = shear force predicted by the proposed model with $2s_c^{\min}$;

V_{H-R} = shear force predicted by Hassan and Rizkalla's model [28]; and

V_{AI} = shear force predicted by Al-Mahmoud et al.'s model [25].

Figures

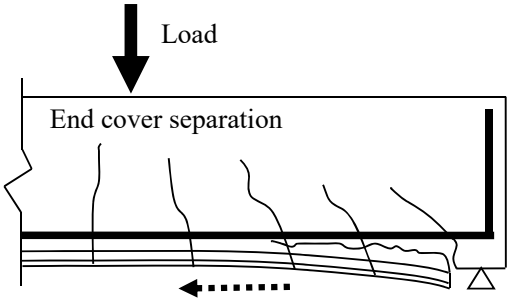

Fig. 1 Schematic of end cover separation

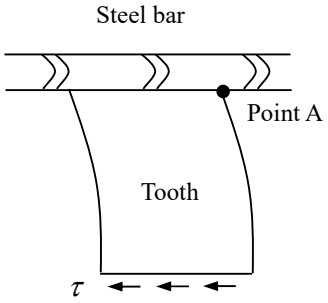

Fig. 2. Concrete tooth between two adjacent cracks

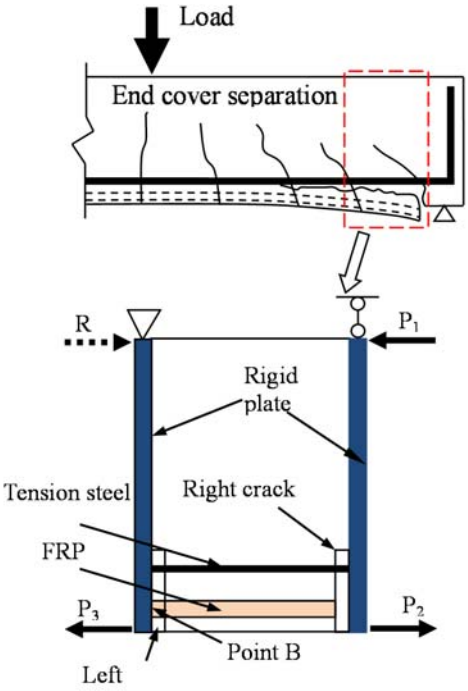

Fig. 3. Simplified finite element model

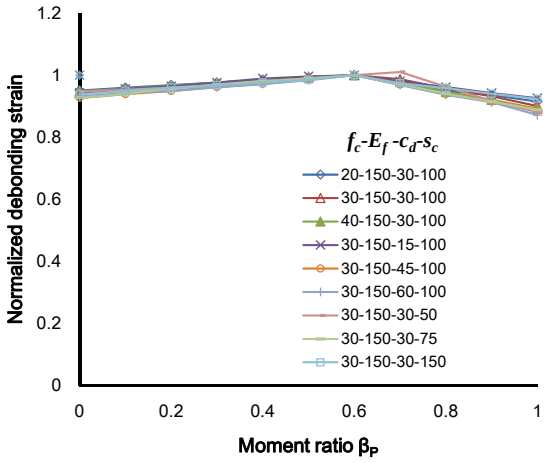

Fig. 4. Effect of moment ratio on normalized debonding strain

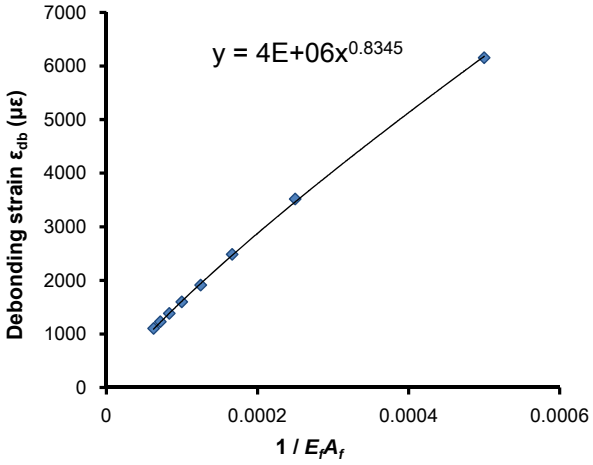

Fig. 5. Effect of axial rigidity of FRP on debonding strain

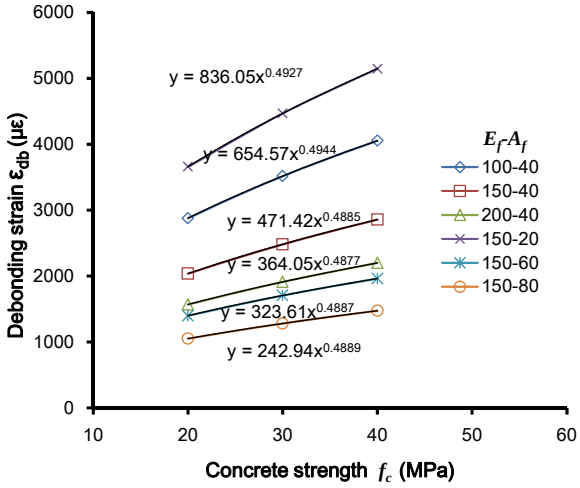

Fig. 6. Effect of concrete strength on debonding strain

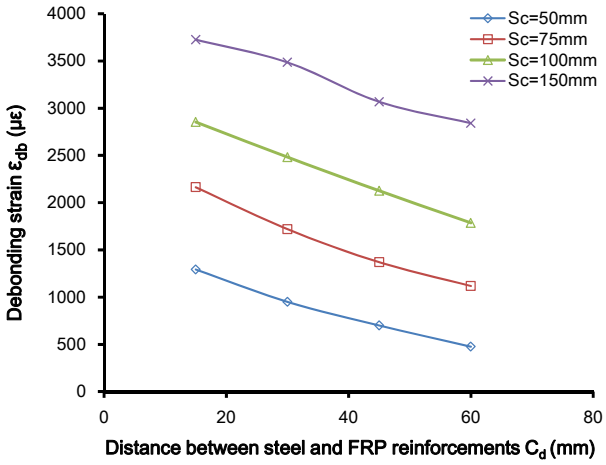

Fig. 7. Effect of distance between steel and FRP reinforcements on debonding strain

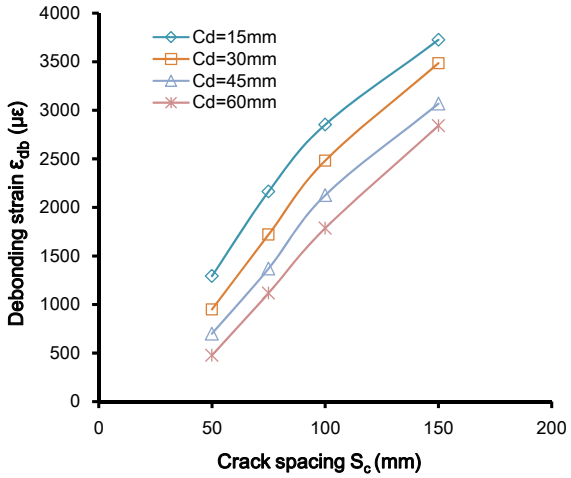

Fig. 8. Effect of crack spacing on debonding strain

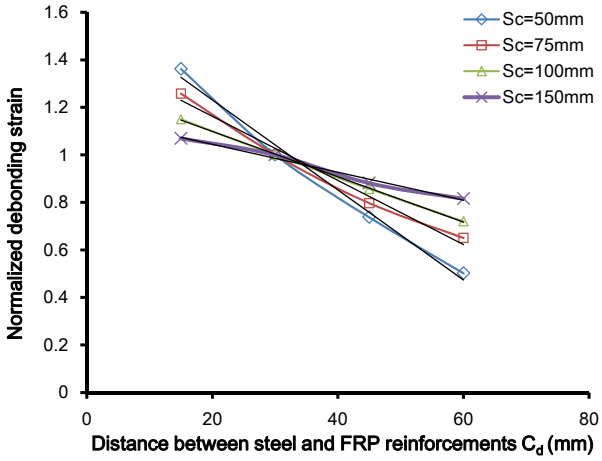

Fig. 9. Effect of distance between steel and FRP reinforcements on normalized debonding strain

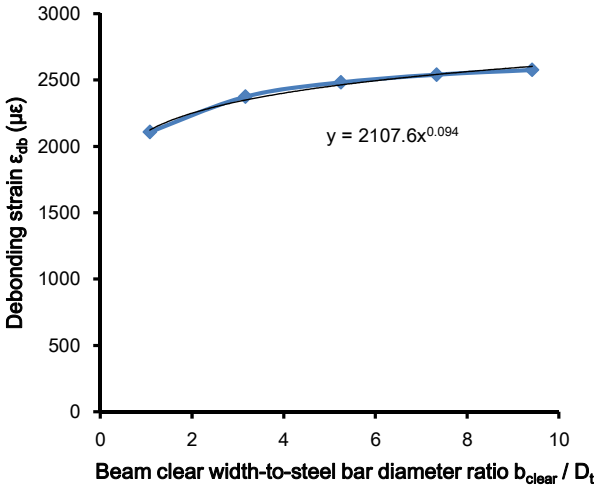

Fig. 10. Influence of beam clear width-to-steel bar diameter ratio on debonding strain

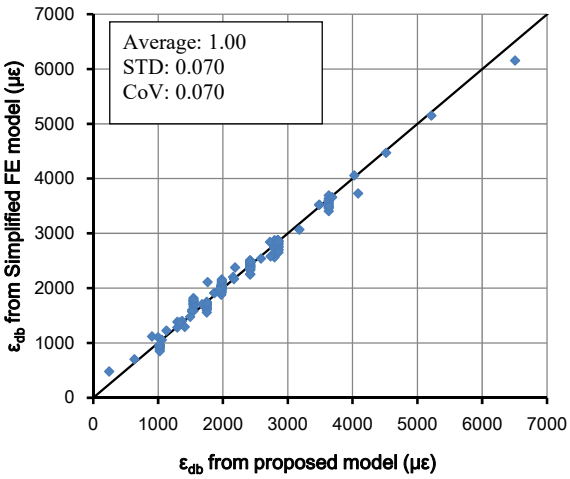

Fig. 11. Comparison of debonding strain between FE predictions and proposed strength model

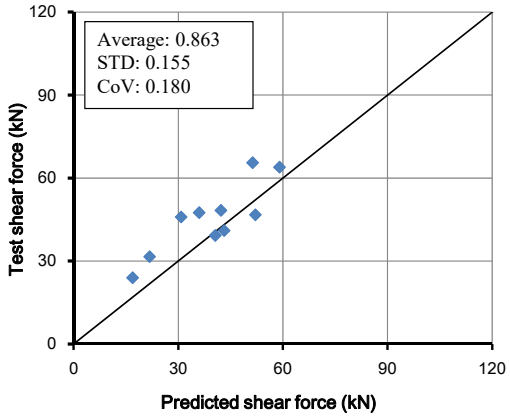

(a) Crack spacing = $s_c^{\min}$

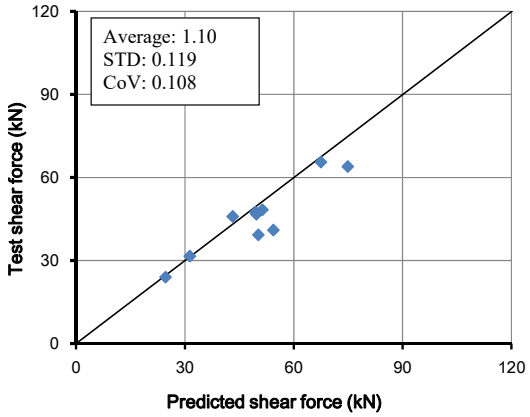

(b) Crack spacing = $1.5s_c^{\min}$

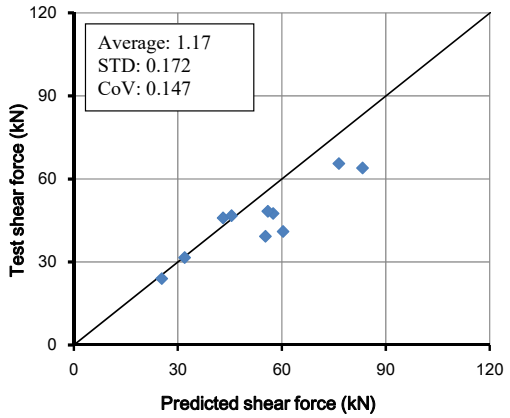

(c) Crack spacing = $2s_c^{\min}$

Fig. 12. Comparison of shear force at debonding between tests and proposed strength model

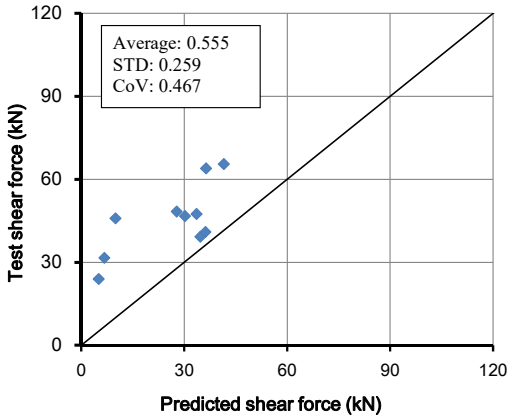

Fig. 13. Comparison of shear force at debonding between tests and Hassan and Rizkalla's model [28]

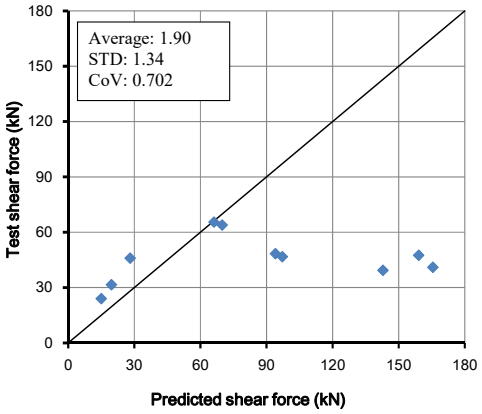

Fig. 14. Comparison of shear force at debonding between tests and Al-Mahmoud et al.'s model [25]